JOURNAL OF AIRCRAFT
Vol. 31, No. 4, July–Aug. 1994

Prediction of Ice Accretion with Viscous Effects on Aircraft Wings

I. Paraschivoiu,* P. Tran,† and M. T. Brahimi‡
Ecole Polytechnique de Montréal, Montréal, Québec H3C 3A7, Canada

A method using the viscous-inviscid interaction technique has been developed for the calculation of ice accretion on three-dimensional wings of any cross section or planform geometry. This technique matches a panel method for external potential calculation with a boundary-layer correction to calculate the flowfield. The resulting velocity field is subsequently used to compute water droplet trajectories and their impact points on the wing to obtain the quantity of ice accumulated. The method yields ice shapes that are in good agreement with numerical and experimental results in rime ice conditions.

Nomenclature

A_{jk} = normal component of the velocity induced at the jth collocation point by the kth surface source
B_{jk} = normal component of the velocity induced at the jth collocation point by the kth bound vorticity
C_D = drag coefficient
C_f = skin-friction coefficient
C_{jk} = normal component of the velocity induced at the jth collocation point by the kth line source
D_{eq} = equivolumetric diameter
D_{jk} = normal component of the velocity induced at the jth collocation point by the kth horseshoe vortex
F = entrainment factor
$\boldsymbol{g}$ = gravitational acceleration vector
h_1, h_2 = metrics of the surface coordinate system
$\boldsymbol{K}$ = Kernel vector
l, m = Thwaites nondimensional parameters
N_d = number of droplets
N_T = total number of singularities
$\boldsymbol{n}_p$ = outward normal vector at point P
q = function of the metrics of the surface
R_e = Reynolds number
R_x = local Reynolds number
u_e = resultant velocity at the edge of boundary layer
$\boldsymbol{V}$ = velocity vector
V_∞ = freestream velocity
v = volume
W_{iw} = transpiration velocity
Γ_h = horseshoe vortex strength
γ = vorticity strength
Δ = mass flow thickness
$\Delta_{1,2}$ = displacement thicknesses in the nonorthogonal curvilinear coordinate system
δ = boundary-layer thickness
δ^* = displacement thickness
η = collection efficiency
θ = momentum thickness
ν = kinematic viscosity
σ = source strength

Presented as Paper 93-0027 at the AIAA 31st Aerospace Sciences Meeting and Exhibit, Reno, NV, Jan. 11–14, 1993; received Jan. 17, 1993; revision received Sept. 13, 1993; accepted for publication Sept. 14, 1993.

*Aeronautical Chair Professor, Department of Mechanical Engineering. Member AIAA.
†Ph.D. Student, Department of Mechanical Engineering.
‡Research Associate, Department of Mechanical Engineering. Member AIAA.

Introduction

OVER the years, the aeronautical industry has developed considerable expertise in the design and conception of the most advanced equipment and systems for a safe and economical aircraft operation. However, the increased need for an aircraft to operate, and thus to be certified, in all weather conditions has presented new requirements. Aircraft must now be tested under icing conditions since ice accretion on unprotected aircraft components can lead to large performance penalties[1] such as increased drag, reduced amount of available lift, decreased stall angle, and increased required engine thrust. Furthermore, the presence of ice on various structures also results in vibration that causes added stress, as on the aircraft components. These different effects account for a loss in aerodynamic and operation efficiency and, more importantly, a reduction in the safety margin during different flight regimes. The aviation certification process for aircraft operating in icing conditions requires extensive flight test analyses that are not only expensive, but also extremely dangerous. Therefore, it is of the utmost importance to develop accurate numerical simulation techniques to predict the growth as well as the shape of ice formed on aircraft components, and more specifically, predict the performance penalties suffered by an aircraft flying in icing conditions. In previous studies, we developed a two-dimensional computer code[2] for ice accretion calculation that was extended to a three-dimensional inviscid code for ice prediction on wings.[3] This code was then matched with a boundary-layer calculation code to take into account the viscous effects. The flowfield calculation uses a viscous-inviscid interaction (VII) technique. In this article, results obtained with the new code, "INTERICE," are presented.

Viscous-Inviscid Interaction Method

The computational procedure for ice accretion calculation is an iterative process where the flowfield calculation influences the ice formation, which in turn, changes the flowfield. The procedure to develop the present code involves three main steps: 1) flowfield calculation, 2) particle trajectory calculation, and 3) ice accretion prediction. In this article, the VII technique has been used.[4] This technique involves a panel method, a boundary-layer correction, and a suitable matching procedure using the transpiration velocity model. The VII technique assumes that the flow can be divided in two separate regions: 1) an external region where the effects of viscosity can be neglected and 2) an internal region near the surface of the wing where viscosity effects must be taken into account. This assumption is certainly valid for many practical applications because the effects of viscosity and turbulence are confined to a thin region near the body surface region, the

boundary layer, and its wake. For the external region, the Euler equations represent a suitable approximation. Two solutions are obtained separately and then are matched in an iterative manner to obtain a final solution to the problem. This method is less time-consuming than the full solution of the Navier-Stokes equations or of wind-tunnel testing. It gives very accurate results. The effect of the boundary layer on the external inviscid flow is simulated by means of an inviscid calculation of the flow over a solid displacement surface. The boundary-layer correction changes the geometry of the surface. A different approach called the transpiration model,[4] in which the displacement effect is simulated by means of a distribution of sources on the true surface of the wing, leads to a nonzero component of the normal velocity there. Thus, for the first calculation of the potential flow, the normal velocity is equal to zero at the body surface. For the subsequent calculations, the boundary conditions of normal velocity at the body surface are modified to obtain a nonzero component. The flowchart in Fig. 1 illustrates this method schematically.

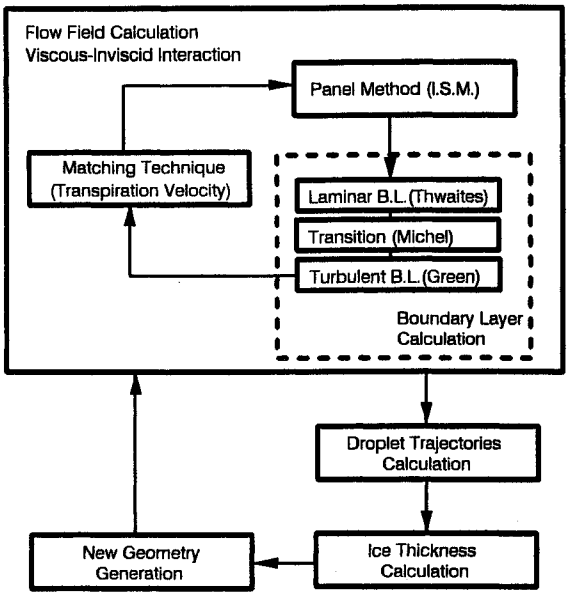

Fig. 1 Flowchart of the ice accretion process.

Internal Singularity Method

The velocity potential of an irrotational and incompressible flow is governed by Laplace's equation, and the flow past a wing can be represented by the sum of different elementary flows. In this article, the internal singularity method (ISM) has been used.[4] This method distributes source and vorticity on the mean camber surface of the wing leaving a small gap near the leading edge. The boundary conditions are satisfied on the wing surface.

In the present calculation scheme, the mean camber surface is designated as S_c, and the wake surface as S_w. The vorticity distribution γ is placed on S_c and S_w, whereas the source distribution is placed on S_c. In addition, two discrete line sources σ_{L_1} and σ_{L_2} are placed on two lines, denoted by L_1 and L_2 in Fig. 2, near the leading edge in the spanwise direction. To complete the singularity model, a set of horseshoe vortices are placed with the bound vortices on a line L_3 halfway between L_1 and L_2, whereas the trailing vortices lie in the streamwise direction along the mean camber surface past the trailing edge and extending downstream into the wake to infinity. The line sources L_1 and L_2, and the bound vortices on L_3, are placed to simulate the rounded shape of the leading edge of a subsonic airfoil.

The equation for the normal velocity of any field point P is obtained by taking the outward normal component of the various induced velocities[4]

$$-4\pi V_\infty \boldsymbol{n}_p = \int\int_{S_c} \sigma_s(\boldsymbol{K}_s \boldsymbol{n}_p)\,dS + \int\int_{S_c+S_w} (\boldsymbol{\gamma} \times \boldsymbol{K}_v)\boldsymbol{n}_p\,dS + \sum_{L_3} (\boldsymbol{K}_{HV}\boldsymbol{n}_p)\Gamma_h + \int_{L_1+L_2} (\sigma_{L_1} + \sigma_{L_2})(\boldsymbol{K}_{LS}\boldsymbol{n}_p)\,dl \quad (1)$$

where the different $\boldsymbol{K}$ vectors represent the appropriate induced fields. The outward normal component of the velocity is zero at the collocation point on the wing surface for the first iteration, but is nonzero for the subsequent equivalent inviscid flow calculations. To obtain the solution for the present inviscid flow calculation, Eq. (1) is solved simultaneously with the Kutta condition. The Kutta condition is satisfied by setting the bound vorticity strength at the trailing edge of the wing to zero. To achieve this objective, the integral equation is discretized to obtain a set of linear algebraic equations. The wing surface is discretized into a number of small elements, panels. The points defining the wing are input in such an order that they define a family of approximately parallel curves lying on the wing surface, designated as N lines as shown in Fig. 2. On a lifting wing, they are oriented in the freestream

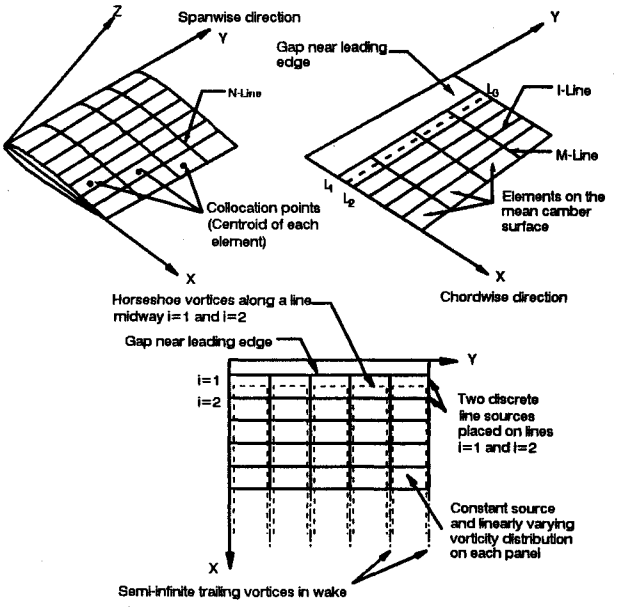

Fig. 2 Discretization of the wing and mean camber surfaces.

direction. On each of the N lines, the points are input beginning at the trailing edge, around the section curve of the wing, and back to the trailing edge. Each N line contains the same number of input points. Points from adjacent N lines are linked to form surface elements. The set of elements formed from two adjacent N lines is designated as a strip of elements. The order in which the points are input is important since it determines the direction of the outward surface normal vector. The normal vector must point into the flowfield. The elements are approximated as plane trapezoids. The centroids of the elements are selected as control points for applying the boundary condition. They are known as collocation points. An extra set of collocation points along the leading edge are also given as input in the definition of the wing geometry. To determine the curve on the mean camber surface, the code calculates the z coordinate of any point on the mean camber surface by averaging the z coordinate of the two corresponding points on the lower and upper surfaces. The curves obtained are designated as M lines. Points on adjacent M lines are linked to form another family of curves, termed as I lines as shown in Fig. 2. The mean camber surface is divided into a number of small elements by these M and I lines.

The integral Eq. (1) can be approximated by a set of linear algebraic equations for the unknown singularity distribution as[4]

$$\sum_{k=1}^{(I-1)(M-1)} A_{jk}\sigma_{sk} + \sum_{k=1}^{(I-1)(M-1)} B_{jk}\gamma_k + \sum_{k=1}^{(M-1)} C_{jk}(\sigma_{L_{1k}} + \sigma_{L_{2k}}) + \sum_{k=1}^{(M-1)} D_{jk}\Gamma_{hk} = -\boldsymbol{n}_j V_\infty$$

$$j = 1, 2, \ldots, 2(I-1)(M-1) \tag{2}$$

where $(I-1)$ and $(M-1)$ are the number of chordwise and spanwise on the mean camber surface. This set of equations is solved to obtain the unknown singularity strengths. Once the solution is obtained the total velocity at any jth collocation point can be calculated according to

$$V_j = \sum_{k=1}^{N_T} V_{jk}\Pi_k + V_\infty \tag{3}$$

where V_{jk} represents the total induced velocity at the jth collocation point due to kth singularity Π_k, and N_T is the total number of singularities.

Boundary-Layer Calculation

The second important component of any VII scheme is the boundary-layer calculation. The calculation of the viscous part of the problem has usually involved the assumptions that the normal pressure gradient across the boundary layer is negligible, and that only the normal derivatives of the shear stresses are important to the calculation.

In the practical range of Reynolds numbers, the flow is predominantly turbulent, but it is still necessary to use a method for the laminar boundary layer ahead of the transition and another method for determining the starting conditions for the turbulent boundary layer. The boundary-layer characteristics are calculated using the strip theory. A two-dimensional boundary-layer calculation is performed on each spanwise section and all variables are supposed constant along a particular spanwise section.

In the present method, the calculation of the laminar boundary layer is based on Thwaites' method.[5] The transition from laminar to turbulent flow is calculated using Michel's criterion,[6] which gives transition in a pressure gradient on the basis of a relation between R_θ and R_x:

$$R_\theta > 1.174[1 + (22400/R_x)]R_x^{0.46} \tag{4}$$

The transition is assumed to be sudden. This criterion enables us to obtain the starting values for the turbulent boundary-layer calculation by assuming that they are equal to the values for the laminar boundary-layer calculation.

An integral method for the boundary-layer calculation solves the Kármán momentum equation

$$\frac{d\theta}{dx} + (H+2)\frac{\theta}{u_e}\frac{du_e}{dx} = \frac{1}{2}C_f \tag{5}$$

where θ, the shape parameter H, δ^*, and C_f, are defined as

$$\theta = \int_0^\infty \frac{u}{u_e}\left(1 - \frac{u}{u_e}\right) dy \tag{6}$$

$$H = (\delta^*/\theta) \tag{7}$$

$$\delta^* = \int_0^\infty \left(1 - \frac{u}{u_e}\right) dy \tag{8}$$

$$C_f = (\tau_w/\tfrac{1}{2}\rho u_e^2) \tag{9}$$

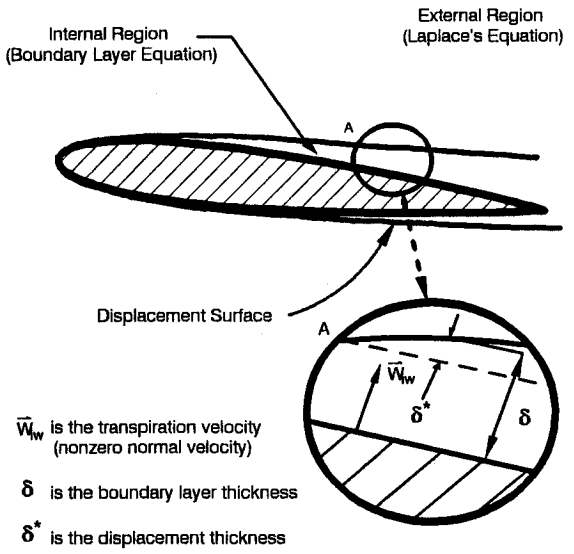

Fig. 3 Details of the boundary-layer region.

With the help of transformation formulas and known exact results, Thwaites[5] found the solution of the Kármán's momentum equation for incompressible flow in the form of a quadrature for the momentum thickness:

$$\frac{\theta^2}{\nu} = \frac{0.45}{u_e^6}\int_0^s u_e^5\, ds \tag{10}$$

The other boundary-layer parameters such as δ^* and C_f can be obtained from Thwaites' table[5] of m, l, and H, which relates these parameters on the assumption of a one-parameter family for velocity profiles using empirical relations.

To calculate the turbulent boundary layer, the lag-entrainment method of Green[7] has been used. This method is based on a model proposed by Head[8] in which the boundary-layer growth is predicted by the simultaneous forward integration of the momentum integral equation and the entrainment equation. The following parameters are defined: Δ, the mass and H_1, another shape parameter. F is the entrainment coefficient and δ is the overall boundary-layer thickness as shown in Fig. 3. The point A is the intersection between the outer streamline and the boundary layer:

$$\Delta = \int_0^\delta \frac{u}{u_e}\, dy = \delta - \delta^* \tag{11}$$

$$H_1 = \frac{\Delta}{\theta} \tag{12}$$

$$F = \frac{1}{u_e}\frac{d}{dx}(u_e\Delta) \tag{13}$$

The von Kármán momentum integral equation may be written

$$\frac{d\theta}{dx} = \frac{C_f}{2} - (H+2)\frac{\theta}{u_e}\frac{du_e}{dx} \tag{14}$$

The entrainment equation, which is an expression for streamwise change of the mass flow thickness, can be written as

$$\frac{d\Delta}{dx} = F - \frac{\Delta}{u_e}\frac{du_e}{dx} \tag{15}$$

By combining Eqs. (14) and (15), we obtain

$$\theta\frac{dH_1}{dx} = F - H_1\left[\frac{C_f}{2} - (H+1)\frac{\theta}{u_e}\frac{du_e}{dx}\right] \tag{16}$$

To integrate these equations, expressions for H, F, and C_f as functions of H_1 and θ must be determined. Head[8] gives empirical relations between the entrainment and skin-friction coefficients and the two shape parameters. These are related to the flat-plate values that are denoted by the subscript 0. Green has replaced Head's relations by closely similar ones that help tie the method to the well-documented case of the boundary layer in zero pressure gradient or flow over a flat plate[7]:

$$C_{f0} = \frac{0.012}{\log_{10}R_\theta - 0.64} - 0.00093 \tag{17}$$

$$H_0 = [1/(1 - 6.8)\sqrt{(C_{f0}/2)}] \tag{18}$$

where R_θ is the Reynolds number based on momentum thickness. The relation between the actual friction coefficient and the shape parameter H and their flat-plate values is given by the expression

$$[(C_f/C_{f0}) + 0.5][(H/H_0) - 0.4] = 0.9 \tag{19}$$

Relations for F and H as a function of H_1 are also needed:

$$F = 0.0299(H_1 - 3.0)^{-0.6169} \tag{20}$$

$$H = 1 + 1.12[H_1 - 2 - \sqrt{(H_1 - 2)^2 - 3}]^{0.915} \tag{21}$$

Transpiration Velocity

Once the boundary-layer calculation is achieved, we calculate the surface transpiration velocity to modify the boundary conditions for the equivalent potential flow calculation. W_{iw} is obtained by integrating the continuity equation with respect to z from 0 to δ. For incompressible flow, we obtain[4]

$$W_{iw} = \frac{1}{q}\left[\frac{\mathrm{d}}{\mathrm{d}x}\left(\frac{u_e\Delta_1 q}{h_1}\right) + \frac{\mathrm{d}}{\mathrm{d}y}\left(\frac{u_e\Delta_2 q}{h_2}\right)\right] \tag{22}$$

The transpiration velocities change the boundary conditions for the equivalent inviscid flow; the velocity and pressure distributions are recalculated for the next boundary-layer calculation. These transpiration velocities are calculated after each five iterations of boundary-layer calculation. The whole calculation technique stops when the difference of the sectional lift coefficients of the wing, in subsequent iterations, is small enough. It is very convenient to use the transpiration velocity model since it has the advantage that, if a panel method is used, the matrix of influence coefficients does not change from iteration to iteration and can be inverted once and stored since the influence coefficients depend only on the geometry, which is constant. Only the right side vector of normal velocities changes with each iteration. The solid displacement model changes the geometry of the body at every iteration and the matrix of influence coefficients must be recalculated. In a panel method, the most time-consuming step is certainly the calculation of the influence coefficients. For this particular advantage, the transpiration velocity model has been chosen.

Particle Trajectory Calculation

Calculation of trajectories is the most time-consuming step in the overall process. This is due to the fact that hundreds of droplets must be followed individually over their entire path. First, the initial droplet position is determined and its new position is recalculated after a time interval Δt. This Δt must be chosen carefully. It must be small enough to yield good accuracy. However, if it is too small, the overall process is lengthened considerably.

To calculate the droplet trajectories, the following assumptions were made:

1) The volume of the droplet remains constant throughout the entire process. However, the droplet may or may not keep its spherical shape. D_{eq} is the diameter that a spherical droplet with equal volume would have.

2) The droplet density ρ_d remains constant throughout the whole path.

3) The initial droplet velocity is equal to V_∞, the droplets are much smaller than the body considered so that they do not affect the velocity field.

To calculate the trajectory of a droplet, we take into account the gravitational, buoyancy, and drag forces. The equation of motion of the droplet is

$$M_d\boldsymbol{a}_d = (\rho_d - \rho_a)v\boldsymbol{g} + \tfrac{1}{2}\rho_a S C_D|\boldsymbol{U} - \boldsymbol{V}_d|(\boldsymbol{U} - \boldsymbol{V}_d) \tag{23}$$

where M_d and $\boldsymbol{a}_d$ are the mass and the acceleration of the droplet, ρ_a and ρ_d the densities of air and water, v the volume of the droplet, $\boldsymbol{U}$ and $\boldsymbol{V}_d$ the velocity vectors of the fluid and the droplet, S the area normal to the freestream direction, and C_D represents the drag coefficient of the droplet. It is assumed that the area S is the area for an equivolumetric sphere and that any deviation from spherical shape is included in the drag coefficient. A droplet moving in the stream will be deformed so that D_{eq} is used. The effects of this deformation are included in C_D. The $(C_D R_e/24)$ coefficient is assumed to only depend on the Reynolds number, and is given by Gunn and Kinzer.[9] The equation relating this coefficient to the Reynolds number is given by

$$(C_D R_e/24) = 1.699 \times 10^{-5}(R_e)^{1.92} \tag{24}$$

The droplet equation of motion is solved using a fourth-order Runge-Kutta numerical integration procedure.

Ice Accretion Prediction

Calculation of the Collection Efficiency

The maximum amount of water that impinges on the wing depends on several parameters. The major parameters are S_F, the normal surface of the wing to the freestream direction, V_∞, and the liquid water content (LWC):

$$\dot{m}_{e,\max} = V_\infty S_F \mathrm{LWC} \tag{25}$$

The true mass flow rate that impinges on the wing is lower because the droplets have a tendency to follow the streamlines sweeping past the obstacle. The water mass flow rate that impinges on the wing is given by

$$\dot{m}_e = \eta V_\infty S_F \mathrm{LWC} \tag{26}$$

where η is the ratio between the area where droplets impinge on the wing and the total frontal area S_F. This coefficient depends on several parameters, including the shape and maximum thickness of the cross section of the wing, the mean equivolumetric diameter (MED) of the droplets, V_∞, and the angle of attack α. The velocity field, with or without ice was already determined using a panel method, and is considered known. The velocity field is used to compute the trajectory of a given droplet to determine whether or not it impinges on the wing.

Calculation of a Particle Impact Point

The droplet impact point calculation can be considered two dimensional since the computation is done on each spanwise section. The computer code determines the first and last impact points on the cross section. These are the farthest points downstream on the upper and lower surfaces where droplets impinge on the airfoil. These two points define an area upstream of the airfoil where the droplets, which are included in this particular area, will impinge at different impact points. This area is divided into a finer mesh that determines the

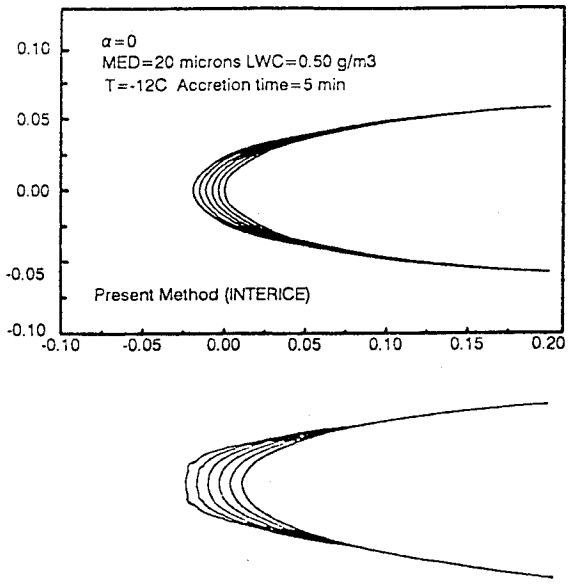

Fig. 4 Comparison of ice accretion with fortified LEWICE code at $\alpha = 0$ deg ($y/b = 0.1$).

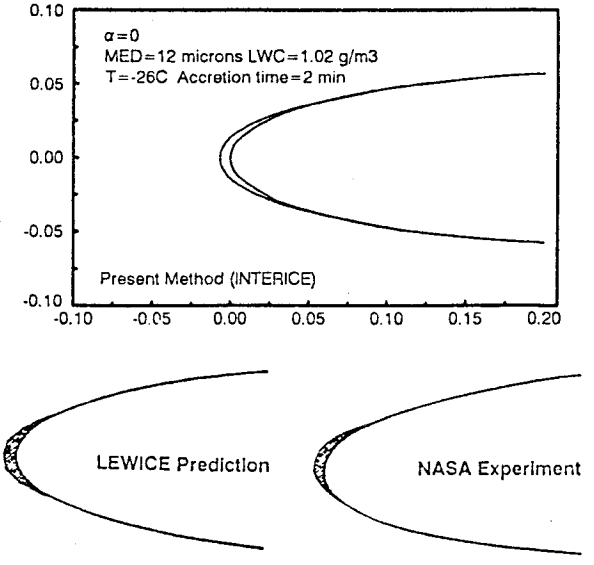

Fig. 5 Comparison of ice accretion with LEWICE and NASA experiment at $\alpha = 0$ deg ($y/b = 0.1$).

accuracy of the computation. A droplet is released at each node of this mesh and its trajectory is calculated in order to determine its impact point. This finer grid is obtained by dividing every panel into 20 subdivisions.

To obtain the impact point of a droplet, we consider that the droplet moves from a point P_1 of coordinates (x_1, z_1) to another point P_2 of coordinates (x_2, z_2), and has a trajectory that can be written in parametric form as

$$x = x_1 + (x_2 - x_1)t_1 \tag{27}$$

$$z = z_1 + (z_2 - z_1)t_1 \tag{28}$$

The equation of each subdivision is also written in parametric form

$$x = x_{(j)} + [x_{(j+1)} - x_{(j)}]t_2 \tag{29}$$

$$z = z_{(j)} + [z_{(j+1)} - z_{(j)}]t_2 \tag{30}$$

where $x_{(j)}$ and $z_{(j)}$ represent the coordinates of the first point of the jth subdivision, t_1 and t_2 represent the geometric pa-

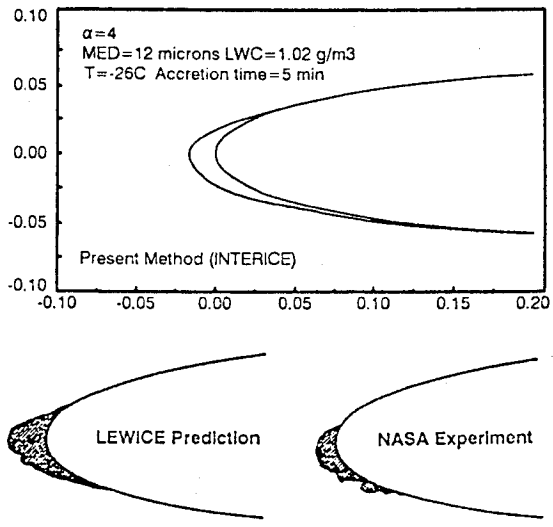

Fig. 6 Comparison of ice accretion with LEWICE and NASA experiment at $\alpha = 4$ deg ($y/b = 0.1$).

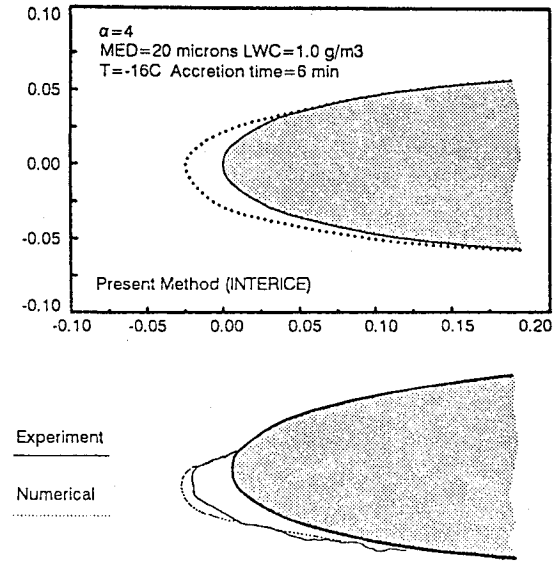

Fig. 7 Comparison of ice accretion with turbulent model for LWC = 1.0 g/m³ at $\alpha = 4$ deg ($y/b = 0.1$).

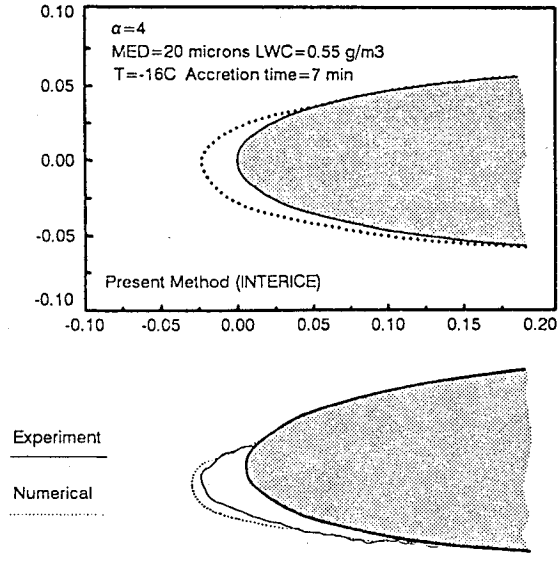

Fig. 8 Comparison of ice accretion with turbulent model for LWC = 0.55 g/m³ at $\alpha = 4$ deg ($y/b = 0.1$).

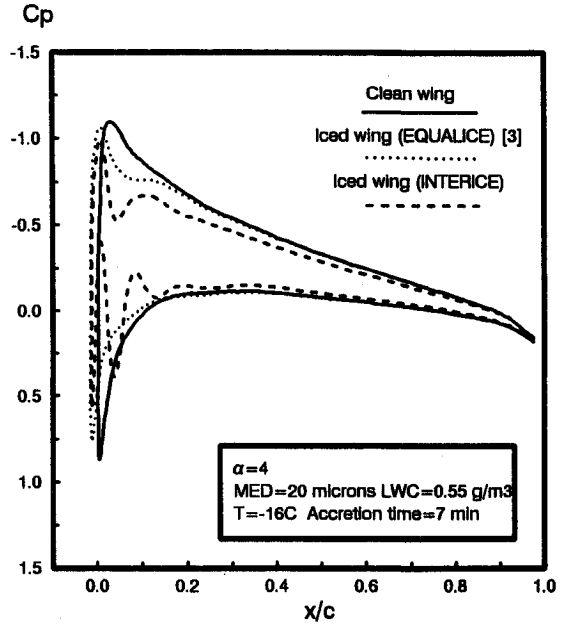

Fig. 9 Pressure distribution on NACA 0012 at $\alpha = 4$ deg and $y/b = 0.1$.

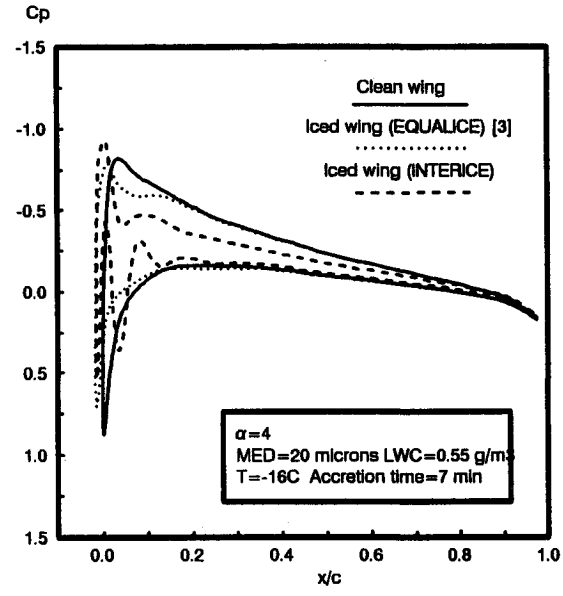

Fig. 10 Pressure distribution on NACA 0012 at $\alpha = 4$ deg and $y/b = 0.9$.

rameters. There is impact on a given subdivision if ($0 \leq t_1 \leq 1$, $0 \leq t_2 \leq 1$).

For every node of the coarser grid, i.e., the original grid, the computer code counts the number of droplets that impinge on the four nearest subdivisions, two subdivisions upstream and two downstream. All the droplets impinging on these four subdivisions are assumed to accumulate directly on this node. The computer code can now calculate the ice thickness at that specific node using the mass flow rate that impinges on the node. The mass flow rate at the node is written as

$$\dot{m}_{e(j)} = \dot{m}_e(N_{(j)}/N_d) \tag{31}$$

where $N_{(j)}$ represents the number of droplets that impinge on that particular node, and N_d represents the total number of droplets that impinge on the airfoil.

Results

To validate INTERICE code, a comparison of the present method with numerical and experimental results given by Cebeci et al.,[10] MacArthur,[11] and Shin et al.[12] has been done for NACA 0012 in rime ice conditions for two angles of attack, $\alpha = 0$ and $\alpha = 4$ deg, and three ambient temperatures: -12, -16, and -26°C. Figure 4 shows rime ice shapes for different ice accretion times at a temperature of -12°C for a zero angle of attack and freestream velocity of 64.73 m/s. The results show that ice formation on the upper and lower wing surfaces are symmetric, and the limit trajectories are about 8% of the chord. After 5 min of ice formation, the maximum ice thickness predicted is in the order of 2% of the chord. These ice shapes predictions look quite different from that given by Cebeci et al.[10] results, since the later were computed for two-dimensional case only. At a temperature of -26°C and ice accretion time of 2 min and a zero angle of attack, Fig. 5, results show also good agreement with MacArthur numerical results, although the lower limit trajectory is not well predicted when compared to NASA experiment. In Fig. 6, results of ice shape after 5 min at an angle of attack $\alpha = 4$ deg are in good agreement for the ice thickness, however, the limit trajectories show some differences with both INTERICE and LEWICE codes. Figures 7 and 8 show a comparison of INTERICE code results with experimental data and numerical results given by Shin et al.[12] at an ambient temperature of -16°C, an angle of attack $\alpha = 4$ deg, and two different ice accretion times, 6 and 7 min, for a freestream velocity of 69 and 102 m/s, respectively. Generally, the present method compares well with both experimental and numerical results for both ice shape and thickness. Figures 9 and 10 present pressure distributions obtained in the same conditions as in Fig. 8. Results obtained with the present method are compared to those obtained with the earlier code without viscous effects,[3] as well as with the clean wing. As expected, the presence of ice on the wing creates important changes near the leading edge, which are more important when the viscous effects are taken into account. We should notice that the results given by INTERICE are valid for rime ice conditions only due to the fact that we neglect the thermodynamic analysis and we assume an instantaneous freezing of the incoming supercooled water droplets as soon as they reach and hit wing surfaces. For glaze ice conditions, which is formed at a temperature around 0°C and high liquid water content, it is necessary to take thermodynamic analysis into account since the behavior of unfrozen surface water has a direct influence on the ice accretion mechanisms, which are strongly dependent on the surface roughness, and the mass transfer at the surface of the wing. In contrast to the rime ice accretion process where the thermodynamic effects are neglected, in glaze ice accretion, the behavior of water on the wing surface becomes the key of the analysis.

Conclusions

The INTERICE code can accommodate any wing planform or cross section. It yields accurate results for ice shapes obtained in rime ice conditions. To increase the accuracy of the ice accretion model, the mass and heat transfer at the surface of the body should be taken into account. This would allow us to calculate the glaze ice that occurs when only a fraction of the water droplets freeze upon impact while the remaining droplets run back along the surface or along existing ice and freeze downstream.

Acknowledgments

This work was prepared in the context of J.-Armand Bombardier Aeronautical Chair. The authors gratefully acknowledge the support provided by Bombardier Inc./Canadair, Montréal, Canada, for this project.

References

[1]Potapczuk, M. G., and Berkowitz, B. M., "Experimental Investigation of Multi-Element Airfoil Ice Accretion and Resulting Performance Degradation," NASA TM-101441, Jan. 1989.

[2]Asselin, M., Prud'Homme, M., and Paraschivoiu, I., "Analyse du Mouvement des Gouttelettes d'eau et Formation de la Glace en Aéronautique," Centre de Développement Technologique de l'École Polytechnique de Montréal, C.D.T. Project-C089/Canadair, Final Rept., Montréal, Canada, Aug. 1990.

[3]Tran, P., Brahimi, M. T., and Paraschivoiu, I., "Effects of Ice Accretion on Aircraft Components," Centre de Développement Technologique de l'École Polytechnique de Montréal, C.D.T. Project C128/Canadair, Final Rept., Montréal, Canada, Aug. 1992.

[4]Tran, P., "Viscous-Inviscid Interaction on Wings at Low Speeds," M.Ing., Dept. of Mechanical Engineering, École Polytechnique de Montréal, Montréal, Canada, April 1992.

[5]Thwaites, B., "Incompressible Aerodynamics," Clarendon Press, Oxford, England, UK, 1960.

[6]Michel, R., "Etude de la Transition sur les Profils d'Ailes," ONERA Rept. 1/1578A, Jan. 1951.

[7]Green, J. E., "Application of Head's Entrainment Method to the Prediction of Turbulent Boundary Layers and Wakes in Compressible Flow," Aerodynamics Dept., Royal Aircraft Establishment, R&M 3788, Farnborough, England, UK, 1976.

[8]Head, M. R., "Cambridge Work on Entrainment," Computation of Turbulent Boundary Layers, *AFOSR-IFP-Stanford Conference Proceedings*, Vol. I, 1968, pp. 188–194.

[9]Gunn, R., and Kinzer, G. D., "The Terminal Velocity of Fall for Water Droplets in Stagnant Air," *Journal of Meteorology*, Vol. 6, Aug. 1949, pp. 243–248.

[10]Cebeci, T., Chen, H. H., and Alemdaroglu, N., "Fortified LEWICE with Viscous Effects," *Journal of Aircraft*, Vol. 28, No. 9, 1991, pp. 564–571.

[11]MacArthur, C. D., "Numerical Simulation of Airfoil Ice Accretion," AIAA Paper 83-0112, Jan. 83.

[12]Shin, J., Chen, H. H., and Cebeci, T., "A Turbulence Model for Iced Airfoils and Its Validation," AIAA Paper 92-0417, Jan. 1992.